

Dear OS editor,

we thank both referees for their response. Here, we provide a response to anonymous referee 1. Below is a marked version of the revised manuscript. Note that the captions of the last two figures

5 have been altered because these were exchanged in the last revision, but the marking of these changes is somewhat cluttered. Apologies for the inconvenience.

Anonymous referee 1:

10 The authors have improved on the text and description of the solutions, however, my main concerns regarding the 2-layer experiments and their interpretation remain. On the other hand, this is an interesting and important topic, and I believe that the authors' work can be published after major revisions.

15 General Comments:

1) The authors interpret the different positions of the front in the western basins in their 2-layer model solutions as being the result of local processes, i.e., inertial terms vs. viscosity. In my view, this interpretation may be correct, however, the experiments are not sufficiently well designed (or 20 at least the analysis is not detailed enough) to proof that. As discussed in the manuscript and the authors' response, there are several competing mechanisms which can determine the position of the front. These mechanisms depend on several parameters including the eastern boundary layer thickness at the island, the magnitude of the jump across the front, and the mechanism allowing for the frontal current (viscosity vs inertial). Ideally, only the latter would change to proof the authors point, 25 but this is not the case. Since the authors want keep their current experiments, i suggest that they either add an in-depth analysis of the experiments (e.g., they could compare their numerical solutions to inviscid, analytical solutions, calculate position of fronts as in Dewar, 1991), or they could reformulate their text to indicate that their described dynamical picture is a valid hypothesis, but acknowledge that their solutions may be interpreted in different ways.

30

Detailed Comments:

1) Lines 148-156: I agree that there is still much to be learned about the LC system. One common 35 conclusions of the studies mentioned in this paragraph appears to be, however, that the continental slope is an essential model component in order to simulate a realistic LC. Specifically, when a model (OGCM or 2-layer model) is forced with a meridional surface density gradient, it does not generate a barotropic eastern boundary current without a continental slope. This is a bit problematic given that the 2-layer model configuration used here has a flat bottom and vertical walls. Please discuss in more detail why you think you do not need to consider the effects of a continental slope.

40

2) Line 193-194: "And why are poleward eastern boundary currents like the LC not found in other basins?" If this is really a central question that you want to address in your paper, you should discuss this issue in more detail, and perhaps attempt an answer in the discussion section. There are, in fact, other poleward eastern boundary currents, e.g., the Slope Current in the North Atlantic and 45 the Iberian Poleward Current. It has been suggested that whether the eastern boundary current is directed pole- or equatorwards depends on the relative strength of the offshore meridional surface density gradient and the coastal winds (e.g., Godfrey and Weaver, 1991: Is the Leeuwin Current driven by Pacific heating and winds? Progress in Oceanography). If you have an alternative explanation, it would be useful to contrast the two ideas.

50

3) Lines 267-281: Perhaps you could give the range of w that results from this buoyancy forcing and also the range of Ekman pumping velocities, to give the reader an idea of the relative strength of

these two forcings? Since you have eliminated the equations for the buoyancy forcing and definition of the constants involved, it might also be helpful to convert the colorbar in Figure 3a into velocity units.

4) Lines 288-296: For the model to equilibrate, it is necessary that the mass transfer w between the layers integrated over the domain is zero. I understand that in your 2-layer model, the model reduces to a 1-layer system in the outcrop region (there are different ways to deal with such an outcrop; 60 please indicate clearly how that occurs in your model version). Thus, it appears (and you also stated that in the original version of the manuscript) that, in case of an outcrop, the w no longer balances over the domain, and the model cannot reach a steady state. Given the structure of the buoyancy forcing and the size and position of the outcrop, this imbalance may be substantial. So, I think you need to back up the claim that the model is close to equilibrium with actual numbers. How does the 65 total upper layer volume change between model years 45-55? It also appears as if the layer-1 volume in the solution shown in Fig. 6b was much less than in Fig. 7. When all solutions were started from the same state of rest, that suggests that the volume change is substantial. Please discuss the effect of different layer-1 volume on the key properties of your solutions.

70 5) Lines 296-298: A statistical steady-state is obtained when the model equilibrates, and not by averaging. I think you want to say that you analyze the model variables averaged over years 45 - 55.

6) Line 475: Change “OCEAN” to “Ocean”

75 Reply:

General comments:

We acknowledge that additional quantitative analysis would be required to prove the proposed 80 dynamic connection and specifically the separation of the hypothesised viscous and inertial regimes. Hence we have rephrased the text both in the abstract and discussion to emphasize that we do not provide a full dynamical explanation of the circulation, but rather introduce a new mechanism for the connection of the ITF, SICC and LC backed up with simulations from two models.

85 Detailed comments:

1) The modeled Leeuwin Current is of purely baroclinic nature and has an undercurrent of equal strength in the lower layer. The simulated eastern boundary current is thus similar to that presented by McCreary et al. (1986), without a continental slope and indeed without barotropic velocity. We 90 included this critical point in the manuscript.

2) The Leeuwin Current admittedly is not the only poleward eastern boundary current. However it is unique in its strength and position in a subtropical ocean, hence flowing against the wind. The text is adjusted to clarify what makes the Leeuwin Current unique. In our proposed mechanism, the Leeuwin Current is driven by pacific winds (forcing the ITF) and the subtropical front in the Indian 95 Ocean. This summary is now included in the discussion.

3) In the hydrostatic model, no direct vertical velocity can be inferred directly from the surface buoyancy fluxes. We have reintroduced the formulation of the surface buoyancy condition in the model configuration.

4) We have included a reference to the vorticity scheme (Arakawa and Hsu, 1990), solved in the 100 model to allow for outcrop. The ‘drift’ of the interface over the averaging years is quantified (between 5 and 10% in all simulations). In the simulation without ‘Pacific’ winds, the mean interface depth is 30m shallower over this period than the inviscid simulation including these winds. This corresponds to a stronger front and baroclinic jet and agrees with the GCM simulations with and without ITF.

5,6) Agreed and implemented

The Connection of the Indonesian Throughflow, South Indian Ocean Countercurrent and the Leeuwin Current

E. Lambert¹, D. Le Bars¹, and W.P.M. de Ruijter¹

¹Institute of Marine and Atmospheric Sciences Utrecht, Utrecht University, the Netherlands

Correspondence to: Erwin Lambert (erwin.lambert@uib.no)

105 **Abstract.** East of Madagascar, the shallow ‘South Indian Ocean Counter Current (SICC)’ flows from west to east across the Indian Ocean against the direction of the wind-driven circulation. The SICC impinges on west Australia and enhances the sea level slope, strengthening the long-shore coastal jet: the Leeuwin Current (LC) which flows poleward along Australia. An observed transport maximum of the LC around 22°S can likely be attributed to this impingement of the SICC. The LC is
110 often described as a regional coastal current that is forced by an offshore meridional density gradient or sea surface slope. However, little is known about the controls of these open ocean gradients. The regional circulation system is embedded in the subtropical ‘super gyre’ that connects the Indo-Pacific Oceans via the Tasman Gateway and the Indonesian Passages. The Indonesian Throughflow (ITF) circulates through the Indian Ocean back into the Pacific south of Australia. This return pathway
115 appears to be partly trapped in the upper layer north of an outcrop line. It is redirected along this outcrop line and joins the eastward flow of the SICC. To study the connection of the basin-scale and the inter-ocean scale dynamics, we apply both an ocean general circulation model and a conceptual two-layer model. Shutdown of the ITF in the models leads to a large decrease in Leeuwin Current transport. Most of the SICC was found to then reconnect to the internal gyre circulation in the Indian
120 Ocean. ITF, SICC and LC ~~are thus thus appear to be~~ dynamically connected.

1 Introduction

In the upper layer of the South Indian Ocean (SIO) three unique anomalous currents have been identified: the Leeuwin Current (LC, Cresswell and Golding (1980)) which flows poleward along Australia; the South Indian Ocean Counter Current (SICC, Palastanga et al. (2007)) which flows
125 from Madagascar to Australia in the upper ± 300 m; and the Indonesian Throughflow (ITF, Godfrey and Golding (1981)) which flows through the Indonesian passages from the tropical Pacific to the Indian Ocean. The LC is unique as an eastern boundary current. Satellite observations show that this is the only eastern boundary region of enhanced mesoscale eddy activity (Schouten et al., 2005; Morrow and Birol, 1998). Across the SIO, the SICC flows against the direction of the wind (curl)

130 driven Sverdrup circulation that moves underneath it. In contrast to other Subtropical Countercurrents (STCCs) which dissolve in the gyre, the SICC spans the full width of the basin. Large vertical shear between these opposing currents leads to (baroclinic) instability and eddies that propagate westward (Palastanga et al., 2007; Jia et al., 2011). The ITF is part of the subtropical ‘super gyre’, a wind-driven circulation which connects the Pacific, Indian and Atlantic Oceans via the Indonesian

135 Passages and the Agulhas and Tasman Gateways (Speich et al., 2007; de Ruijter, 1982; Ridgway and Dunn, 2007). Hypotheses on the nature and coherence of this shallow circulation system range from localized frontal jets to a system that connects the Indonesian Throughflow, the Mozambique Channel and Agulhas Current, the SICC and the Leeuwin Current System. In this study, we provide evidence supporting this latter theory of a large-scale connectivity.

140 Most studies of the Indian Ocean have been complementary in focusing on either the western or the eastern sector. Observations in the west have suggested the Agulhas Retroflection and Return Current as the origin of the SICC (Nauw et al., 2008). In the east, observations (Smith et al., 1991; Woo et al., 2006; Woo and Pattiarrachi, 2008; Weller et al., 2011) and Lagrangian models (Song et al., 2004; Domingues et al., 2007; Valsala and Ikeda, 2007; van Sebille et al., 2014) have identified

145 both tropical (including ITF) and subtropical waters as a source for the LC. Basin-wide observations indicate that westward flow around 10°S (partly ITF) and eastward flow near 25°S (SICC) cross the entire basin of the Indian Ocean (see Fig. 1). These findings indicate a large-scale connectivity between the east and west. However, understanding of the dynamics and connection between these shallow currents, the LC, the SICC and the ITF, is still limited.

150 The Leeuwin Current plays an important role in regional climate and ecology (Waite et al., 2007). Linear theory cannot explain such a poleward boundary current along an eastern boundary. Early studies have pointed at observed meridional gradients in density and steric height as a forcing agent for the LC and the influence of the ITF in reinforcing these gradients (Godfrey and Ridgway, 1985; Weaver and Middleton, 1989). Theories on the coastal trapping of the LC have focused on vertical diffusion of Rossby waves (McCreary et al., 1986) and interaction with the continental shelf (Csanady, 1978, 1985). An ongoing program is evaluating these various proposed mechanisms (Furuue et al., 2013; Benthuyzen et al., 2014), but leave the problem of large-scale forcing and connectivity of the LC unanswered. To understand this large-scale forcing, one needs to understand the origin of the off-shore meridional gradients, which hints to an important role of the SICC.

155 The SICC shows similarities to other Subtropical Countercurrents (STCCs) which have been identified in the North Pacific (Uda and Hasunuma, 1969), South Pacific (Merle et al., 1969), North Atlantic (Reid and Mantyla, 1978) and the South Atlantic (Tsuchiya, 1985). These zonal currents have the clearest signature near 20-25°N/S in the western part of the basins. Suggested driving mechanisms are Ekman convergence (Takeuchi, 1984), isothermal convergence (Cushman-Roisin, 1984),

160 shock formation of mixed-layer depth (de Ruijter, 1983), convergence of Rossby waves (Dewar, 1991) and mode water formation (Kobashi and Kubokawa, 2012). No single mechanism has been

identified as the dominant one and all may play a part in the actual frontogenesis forming these STCCs. All studies do, however, agree that the combination of buoyancy forcing and wind stress convergence establishes the observed zonally oriented fronts with associated baroclinic frontal jets.

170 Because these fronts are expressed in a sharp gradient of isopycnal depth (Fig. 2), these isopycnals can outcrop along the fronts of the STCCs. In the southeast Indian Ocean, these forcing components vary clearly at seasonal, interannual and decadal time scales, as shown elegantly by Jia et al. (2011) using a variety of satellite data. They also showed the associated modulation of baroclinic instability and eddy kinetic energy (Palastanga et al., 2007; Jia et al., 2011).

175 The Indonesian Throughflow, due to its advection of warm and fresh water, affects the hydrography in the South Indian Ocean. The effect on the circulation was first studied by Hirst and Godfrey (1993), who performed simulations using a General Circulation Model (GCM). In one run, they applied realistic bathymetry; in a second run, the Indonesian Passages were closed. In the first run allowing the ITF, a shallow southeastward jet appeared near the latitude where the SICC is observed, 180 down to the southwestern tip of Australia. In the second run, blocking of the ITF weakened this shallow circulation. They suggested that the Leeuwin Current System (LCS) is part of this shallow circulation. A model-intercomparison study of three models of varying complexity supported their conclusions (McCreary et al., 2007), yet both studies were based on coarse resolution simulations. The response of the narrow SICC and LC could therefore not be addressed. Le Bars et al. (2013) 185 were the first to perform comparable simulations, with open and closed Indonesian Passages, using a GCM at eddy-resolving resolution. Since analysis of these model results was restricted to barotropic circulation, no conclusions could be drawn on the SICC and LC systems. We will use these data to revise the effect of the ITF on the ‘realistically’ simulated SICC and LC.

190 Three shallow currents have been identified in the South Indian Ocean: the Leeuwin Current, the South Indian Ocean Countercurrent and the Indonesian Throughflow. In this study, we aim to understand if and how these currents form a connected system. We primarily focus on the LC and the SICC and address following questions: What is the dynamic connection between the SICC and the LC? How can the general features of the shallow circulation in the SIO be understood from surface forcing? What is the role of the ITF in this system? And why are poleward eastern boundary 195 currents like of similar strength to the LC not found in other subtropical basins?

200 To answer these questions, two models of different complexity were used. First, an ocean GCM is run at high and coarse resolution to validate against the results of Hirst and Godfrey (1993) and to show the impact of inertia on the sensitivity of the LC and SICC to the ITF. Second, a conceptual regional two-layer model is used to simulate the general shallow circulation features of the SIO from surface forcing and to reveal the sensitivity of these features to removal of the Pacific influence through the ITF. In Sect. 2, properties and configuration of both models are presented. Model results are presented in Sect. 3. With both models, sensitivity of the circulation to the ITF is presented in Sect. 4, which is followed by concluding remarks in Sect.5.

2 Model configurations

205 Two models were used in this study on the dynamics of the shallow circulation in the South Indian Ocean, an ocean GCM and a conceptual two-layer model. In this section, we describe the basic properties and the configuration of both models.

2.1 General Circulation Model: Parallel Ocean Program

210 The Parallel Ocean Program (POP, Dukowicz and Smith (1994)) is an ocean-only general circulation model solving the primitive equations on a horizontal grid with an average resolution of 0.1° and 42 vertical layers. The atmospheric state and precipitation were taken from the CORE dataset (Large and Yeager, 2004), wind stress was computed offline using Hurrell Sea Surface Temperature climatology (Hurrell et al., 2008) and evaporation and sensible heat flux were calculated online.

215 For the GCM analysis, we used data from the simulations performed by Le Bars et al. (2013). After a spin-up of 75 years as described by Maltrud et al. (2010), two simulations were performed: one with realistic bathymetry; and one with closed Indonesian Passages in a similar fashion as Hirst and Godfrey (1993). Both were run for another 105 model years of which the last 50 years of simulation were averaged to approximate a steady state. Simulations were repeated on a horizontal grid with average resolution of 1.0° allowing for validation against previous modeling studies.

220 2.2 Conceptual model: Hallberg Isopycnal Model

225 The Hallberg Isopycnal Model (HIM, Hallberg (1997, 2000)) is a regional ocean-only model solving the hydrostatic primitive equations in spherical coordinates on an Arakawa C-grid. ~~It Using the vorticity scheme of Arakawa and Hsu (1990), the model allows for arbitrarily thin layers and hence admits isopycnal outcrop. The model~~ is configured to an idealized representation of the Indian and Pacific Oceans with horizontal resolution of $0.2 \times 0.2^\circ$, separated by an elongated island representing Australia (Fig. 3). A minimum of idealized forcing terms is applied to simulate a mid-ocean eastward jet in the western basin, and a westward jet along the northern boundary of Australia with a predictable return pathway. These jets will be interpreted as the SICC and the ITF respectively.

230 The model eastern basin is scaled down compared to the actual Pacific Ocean; by adjusting the wind stress amplitude, the model can simulate a realistic Pacific Sverdrup transport. The flat bottom is at a depth of 1500m below the free surface, which is the approximate depth of the wind-driven circulation. An elongated island is chosen to represent Australia. A two-layer system allows for representation of the baroclinic structure of the Indian Ocean. As ~~shown by McCreary et al. (1986)~~, ~~such a configuration with vertical walls is able to produce a poleward eastern boundary current,~~ ~~although it cannot sustain a barotropic transport. As~~ initial state, the interface depth between these layers was taken uniformly at 100m, a typical depth of both the SICC and LC.

Stratification of the model is based on the 20°C isotherm (Fig. 2), determined using Argo float data from the ARIVO project (Gaillard and Charraudeau, 2008) over the corresponding domain and depths. Density of the lower layer is taken as the average density between the isotherm and 240 1500m depth. The respective densities are $\rho_1 = 1029.0$ and $\rho_2 = 1031.6 \text{ kg m}^{-3}$. After spin-up, as described below, the mean interface depth is 200m, giving mean depths of the layers $H_1 = 200$ and $H_2 = 1300 \text{ m}$. This gives an internal Rossby radius of 22 km.

To investigate both inertial and viscous response in the boundary layer regions, we applied two values for horizontal Laplacian viscosity: $A_H = 100$ and $10^4 \text{ m}^2 \text{s}^{-1}$, giving a boundary layer scale 245 of 20 and 80 km respectively. The viscous regime may be compared to coarse simulations from previous studies (Hirst and Godfrey, 1993; McCreary et al., 2007). Along the lateral boundaries we applied no-slip conditions.

The temperature structure in the Indian Ocean clearly reflects the meridional gradient in surface heat flux (Fig. 2). To simulate the effect of surface heating and cooling and freshwater fluxes, we 250 applied a total buoyancy flux, as in Haney (1971), [prescribing a surface boundary condition](#):

$$\frac{B\rho_0}{g} = -K_v \frac{\partial \rho}{\partial z}. \quad (1)$$

Here, B is the surface buoyancy flux in $\text{m}^2 \text{s}^{-3}$. The maximum applied value for B of $12 \times 10^{-9} \text{ m}^2 \text{s}^{-3}$ is equivalent to a surface heat flux of 31 W m^{-2} , a moderate value compared to estimates by Haney (1971). The applied buoyancy forcing has a constant meridional gradient and is independent on longitude (Fig. 3). The total buoyancy [forcing flux](#) is conserved over the ocean surface.

Wind stress is applied separately over two regions. In the western basin (grey hatches in Fig. 3), a sinusoidal wind stress is applied, corrected for curvature due to the spherical coordinates. This forces a single Sverdrup gyre west of the island. In the eastern basin (black hatches in Fig. 3), a wind stress with constant curl is applied, again corrected for curvature. This pattern forces a constant northward 260 Sverdrup transport of 15 Sv, which circulates along the northern, western and southern boundaries of the basin. The westward flow along the northern boundary represents the ITF in this model.

The combined forcing of buoyancy fluxes and wind stress can induce frontogenesis, resulting in outcrop of the interface. This effectively reduces part of the basin to a one-layer system which has to equilibrate laterally. After 50 model years, total energy in the system was found to be approximately 265 constant. [A statistical steady-state was obtained by averaging over the period between model years 45 and 55. We therefore averaged the output over model years 45–55 to resemble a quasi-steady state. Over this period, the mean interface depth increased by 5–10% in each model run as a result of the energy imbalance.](#)

Linear theory allows for qualitative prediction of the resulting circulation, and it is instructive to do 270 so before analysing the results. The applied wind pattern drives a depth-integrated circulation which is a combination of a Sverdrup gyre in the western basin and a jet-like circulation along the northern,

western and southern boundaries, connecting to a broad constant northward flow in the eastern basin. The meridional gradient in buoyancy fluxes produces a baroclinic structure of eastward flow in the upper layer and westward flow in the lower layer, according to thermal wind balance:

$$275 \quad \frac{\partial u}{\partial z} = \frac{g}{\rho_0 f} \frac{\partial \rho}{\partial y}. \quad (2)$$

Here, u is the zonal velocity in ms^{-1} . Frontogenesis can reinforce this meridional gradient (de Ruijter, 1983; Takeuchi, 1984; Cushman-Roisin, 1984), narrowing and enhancing the baroclinic structure, making the eastward flow in the upper layer more jet-like as the observed SICC.

3 Results

280 In the two-layer solutions, the eastward current appears to be connected to the interface outcrop. The basic structure of the circulation is that of a gyre in each of the basins with a super-gyre wrapping around it and flow through both basins (e.g. Pedlosky et al., 1997)). This is what one can see in the northern strip, between 10 and 15°S (Fig. 5b) where the wind forcing in the eastern basin is set to zero, but buoyancy forcing drives a 3 Sv gyre. The mismatch with the Indian Ocean gyre is 285 corrected in a zonal boundary layer west of the northern termination of the ‘island’. At this value of the viscosity parameter, a large part of the northern Pacific inflow makes an excursion along the northern boundary into the western boundary layer of the Indian Ocean (Agulhas), then back northward in a gyre-like flow in the interior of the IO and eastward in the free zonal boundary layer and exiting through the gateway north of the island.

290 Adding the ITF (and thus also the mismatch) by adding northward forcing wind curl over the ‘Pacific’ has much impact on the flow in the eastern IO (Fig. 7b). The zonal front strengthens and the mean interface is 30m deeper than in absence of wind stress in the eastern basin. Consequently, the zonal eastward jet at $\pm 35^\circ\text{S}$ gets stronger and continues-is found to continue straight to the island due to the larger inertia, then southward (as a Leeuwin Current) and exits around the southern tip 295 into the Pacific western boundary layer. Part of it stays in the IO and flows north-eastward where it connects to the SEC and SECC system.

In the case with larger viscosity (Fig. 7a), the free boundary layer flow west of the southern part of the island curves toward and around the southern tip. North of the island, the wider viscous boundary layer now fills the gateway and blocks the IO flow to exit through the northern passageway.

300 Almost all flow entering through the northern passage can only exit south of ‘Tasmania’. The jet-like structure of these zonal boundary layers induces the interface outcrop and associated fronts.

Steady state solutions of the GCM simulations show a shallow current system in the viscous regime (Fig. 4a). The corner shape geometry of south Australia-Tasmania induces a jump in Sverdrup transport across the corner’s latitude. That is matched by a viscous free boundary layer structure with

305 westward flow south of the discontinuity and eastward north of it. At eddy-resolving resolution this is much clearer (Fig. 4b) and here, a compact poleward flowing Leeuwin Current emerges.

Both GCM simulations show a zonal flow east of Madagascar, fanning out broadly in the viscous case east of 90°E while bifurcating into several branches in the eddy resolving case. This is the SICC-system. A similar structure has recently been identified and analyzed from observations (e.g.

310 Menezes et al., 2013).

The northern branch of the model-SICC reaches the North-West shelf, where it feeds into the coastal jet. The southern branch reaches Australia just south of the North West Cape (NWC). Cross-shore transects, taken at regular intervals of 2° along the west-Australian coast, reveal that the LC transport (Fig. 5) upstream of the NWC (22°S, transect F) is low. A sharp increase is found from 315 approximately 0.5 to 2.5 Sv just south of the NWC. This is the latitude of maximal SICC-strength and it suggests that the SICC directly connects to the LC and, in fact, largely determines its strength and existence.

As expected, the viscous circulation (Fig. 7a) shows features similar to those found in the coarse resolution GCM results. A boundary current flows east and eventually bends southeastward to converge 320 toward the southwestern point of the island as described below. This leads to large values of velocity shear along this outcrop line, baroclinic instability and the formation of mesoscale eddies (Palastanga et al., 2007).

To resolve the inertial regime, the simulation was repeated with a smaller lateral viscosity of 100 m^2s^{-1} (Fig. 7b). Due to rectification of the associated modes, the mid-ocean jet flows almost zonally 325 toward the western coast of the island. Against the boundary, it sets up a pressure gradient and induces a coastally trapped poleward current, much like the observed Leeuwin Current. To simulate a Leeuwin Current in a regional coastal model, McCreary et al. (1986) were the first to prescribe an offshore meridional gradient in surface density of approximately 3 kgm^{-3} over a meridional extent of 2000 km. They based this value on observations, and a similar meridional density gradient is 330 found in our eddy-resolving GCM simulations.

Local frontogenesis at gyre-scale is stimulated by Ekman transport convergence. That alone would converge the upper layer to the zero wind stress curl line at 35°S. Negative buoyancy forcing (cooling, evaporation) in the south produces mixed layer deepening and deceleration of the meridional Ekman velocity. That accelerates the convergence and leads to front formation closer to the equator 335 than the Ekman convergence line as resolved by the GCM simulations (Fig. 4b).

4 Sensitivity to Indonesian Throughflow

Hirst and Godfrey (1993) studied the effect of the ITF by artificially closing the Indonesian Passages. This reduced the shallow eastward jet and the transport in the LCS; these results were reproduced with our GCM at coarse resolution (not shown). At eddy-resolving resolution, closure of the Indone-

340 sian Passages significantly reduces the transport through both the SICC and the LC, as can be seen in Fig. 5a. More importantly, this blocking of the ITF breaks up the connection between the modeled SICC and LC.

In the conceptual two-layer model, we applied an unconventional method of ITF simulation by wind forcing only over the eastern sector of the ‘Pacific’. In that way, inflow from the Pacific can 345 be set to zero without geometrically closing the passages. Closing this passage, as was done in the GCM simulations, essentially changes the topology of the basin. The lack of an ITF gateway induces a southward western boundary current in the eastern basin and could generate leakage south of the island, similar to Tasman Leakage, which increases due to blocking of the ITF in the GCM model (Le Bars et al., 2013). The resulting circulation without wind stress over the eastern basin 350 (Fig. 5b) shows a decreased transport along the mid-ocean front. Moreover, the connection between the western and eastern boundary currents is broken.

Without inflow from the eastern basin (ITF), the frontal jet (SICC) merges into the IO-gyre. That would be similar to the positioning of the subtropical countercurrents in other basins. Connection with a poleward EBC (the Leeuwin Current) requires circulation around the island. When inflow 355 from the eastern to the western basin is allowed along the north of the island, part of this island circulation is trapped in the upper layer by limited diapycnal transport. It follows the southern boundary of this upper layer, being the outcrop line.

The evidence collected here supports a view that there is no direct connection of the ITF to the LC. Rather, these currents are connected via the IO western boundary layer (Agulhas) and the SICC. 360 The ITF transport that enters the IO in the north-east and is forced by the wind over the upper layer east of the island, has to exit along the southern boundary of this upper layer. The positioning of this boundary is controlled by the wind pattern in combination with the location of the island. That determines the frontal outcrop line and the Leeuwin Current transport jump when the SICC flows into it. The depth-integrated transport agrees with linear theory and follows the western boundary layer 365 all the way to the latitude of zero wind curl in the eastern basin, which is the southern boundary (not shown). To meet these requirements, transport in the lower layer produces a flow against the shallow SICC-LC system, which is in agreement with observations where a Leeuwin Undercurrent is found, as well as a westward flow in the sub-thermocline Indian Ocean.

5 Conclusions

370 The GCM experiments reported here show that the basic structure of the flow in the south Indian Ocean is linked to the specific corner-shaped geometry of Australia and Tasmania. Integrating the wind-stress curl westward starting at the eastern boundary to determine the Sverdrup transport in the basin, a transport jump results at the southwest corner of Australia. A free zonal boundary layer to the west of the jump matches the unequal Sverdrup regimes (Fig. 4). To the south it is connected

375 with the Agulhas Return Current. The northern edge of the boundary layer is a high shear zone with eastward flow and potential outcropping of the upper layer. This establishes the SICC and its pathway is largely imposed by the basin geometry combined with the wind pattern.

The wind-driven circulation of the Indonesian Throughflow resides partly in this upper layer and this fraction is redirected along the front to flow zonally towards the west coast of Australia. Coming 380 in in the north, it merges and retroflects largely with the Agulhas Current and adds to the zonal jet. In case of outcrop, it is steered to the north of it, across the Indian ~~Ocean~~Ocean and feeds into the Leeuwin Current. The circulation around Australia, driven by Pacific winds, and the subtropical front in the Indian Ocean can thus account for this anomalously strong poleward eastern boundary current. The experiments with the two-layer conceptual model lend support to this interpretation.

385 ~~Two regimes were identified for this connection with the Australian coast~~Both models appear to show two qualitatively distinct regimes of flow: a viscous regime, where the zonal flow bends southward towards the southwestern point of Australia, and no boundary current could be sustained; and an inertial regime, where the front crosses the Indian Ocean zonally, and the jet reaches the coast near the latitude where it departs Madagascar and feeds the Leeuwin Current. Although Ekman 390 transport can redirect the Indonesian Throughflow directly into the Leeuwin Current, a process that accounts for the latter's relatively tropical structure, it cannot explain the forcing of the Leeuwin Current. However, more analysis would be required to fully describe the dynamics governing the front position and its coastal trapping.

This system flows around the island circulation of Madagascar and is modified also by buoy-395ancy fluxes at the surface. Local zonal jets may result from Ekman convergence and mixed layer deepening. However, it is beyond the present study to cover all details of this complex system.

Acknowledgements. Data from *MDT_CNES-CLS13* were produced by *CLS* Space Oceanography Division and distributed by *Aviso*, with support from *Cnes* (<http://www.aviso.altimetry.fr/>). The authors thank Michael Kliphus (IMAU-UU) for the support with running both models.

400 **References**

Arakawa, A. and Hsu, Y.-J. G.: Energy conserving and potential-ensrophy dissipating schemes for the shallow water equations, *Monthly Weather Review*, 118, 1960–1969, 1990.

BenthuySEN, J., Furue, R., McCreary, J. P., Bindoff, N. L., and Phillips, H. E.: Dynamics of the Leeuwin Current: Part 2. Impacts of mixing, friction, and advection on a buoyancy-driven eastern boundary current over a shelf, 405 *Dynamics of Atmospheres and Oceans*, 65, 39–63, doi:10.1016/j.dynatmoce.2013.10.004, <http://dx.doi.org/10.1016/j.dynatmoce.2013.10.004>, 2014.

Cresswell, G. and Golding, T.: Observations of a south-flowing current in the southeastern Indian Ocean, *Deep Sea Research Part A. Oceanographic Research Papers*, 27, 449–466, doi:10.1016/0198-0149(80)90055-2, 1980.

410 Csanady, G. T.: The Arrested Topographic Wave, doi:10.1175/1520-0485(1978)008<0047:TATW>2.0.CO;2, 1978.

Csanady, G. T.: “Pycnobathic” Currents over the Upper Continental Slope, doi:10.1175/1520-0485(1985)015<0306:COTUCS>2.0.CO;2, 1985.

Cushman-Roisin, B.: On the Maintenance of the Subtropical Front and its Associated Countercurrent, *Journal 415 of Physical Oceanography*, 14, 1179–1190, 1984.

de Ruijter, W.: Asymptotic Analysis of the Agulhas and Brazil Current Systems, doi:10.1175/1520-0485(1982)012<0361:AAOTAA>2.0.CO;2, 1982.

de Ruijter, W. P. M.: Frontogenesis in an Advective Mixed-Layer Model, *Journal of Physical Oceanography*, 13, 487–495, 1983.

420 Dewar, W. K.: Arrested fronts, vol. 49, doi:10.1357/002224091784968576, 1991.

Domingues, C. M., Maltrud, M. E., Wijffels, S. E., Church, J. a., and Tomczak, M.: Simulated Lagrangian pathways between the Leeuwin Current System and the upper-ocean circulation of the southeast Indian Ocean, *Deep-Sea Research Part II: Topical Studies in Oceanography*, 54, 797–817, doi:10.1016/j.dsr2.2006.10.003, 2007.

425 Dukowicz, J. K. and Smith, R. D.: Implicit free-surface method for the Bryan-Cox-Semtner ocean model, *Journal of Geophysical Research*, 99, 7991–8014, doi:10.1029/93JC03455, 1994.

Furue, R., McCreary, J. P., BenthuySEN, J., Phillips, H. E., and Bindoff, N. L.: Dynamics of the Leeuwin Current: Part 1. Coastal flows in an inviscid, variable-density, layer model, *Dynamics of Atmospheres and Oceans*, 63, 24–59, doi:10.1016/j.dynatmoce.2013.03.003, <http://dx.doi.org/10.1016/j.dynatmoce.2013.03.003>, 2013.

430 Gaillard, F. and Charraudeau, R.: New climatology and statistics over the global ocean, *MERSEA del*, 5, 2008.

Godfrey, J. S. and Golding, T.: The Sverdrup Relation in the Indian Ocean, and the Effect of Pacific-Indian Ocean Throughflow on Indian Ocean Circulation and on the East Australian Current, *Journal of Physical Oceanography*, 11, 771–779, 1981.

Godfrey, J. S. and Ridgway, K. R.: The Large-Scale Environment of the Poleward-Flowing Leeuwin 435 Current, Western Australia: Longshore Steric Height Gradients, Wind Stresses and Geostrophic Flow, doi:10.1175/1520-0485(1985)015<0481:TLSEOT>2.0.CO;2, 1985.

Hallberg, R.: Time Integration of Diapycnal Diffusion and Richardson Number-Dependent Mixing in Isopycnal Coordinate Ocean Models, *Monthly Weather Review*, 128, 1402–1419, doi:10.1175/1520-0493(2000)128<1402:TIODDDA>2.0.CO;2, 2000.

440 Hallberg, R. W.: HIM: The Hallberg Isopycnal Coordinate Primitive Equation Model, NOAA Geo-physical Fluid Dynamics Laboratory Tech. Report, http://www.gfdl.gov/cms-filesystem-action/user_files/rwh/him_description.pdf, 1997.

445 Haney, R. L.: Surface Thermal Boundary Condition for Ocean Circulation Models, doi:10.1175/1520-0485(1971)001<0241:STBCFO>2.0.CO;2, 1971.

Hirst, A. C. and Godfrey, J. S.: The Role of Indonesian Throughflow in a Global Ocean GCM, *Journal of Physical Oceanography*, 23, 1057–1086, doi:10.1175/1520-0485(1994)024<1895:TRTASC>2.0.CO;2, 1993.

Hurrell, J. W., Hack, J. J., Shea, D., Caron, J. M., and Rosinski, J.: A new sea surface temperature and 450 sea ice boundary dataset for the community atmosphere model, *Journal of Climate*, 21, 5145–5153, doi:10.1175/2008JCLI2292.1, 2008.

Jia, F., Wu, L., and Qiu, B.: Seasonal Modulation of Eddy Kinetic Energy and Its Formation Mechanism in the Southeast Indian Ocean, *Journal of Physical Oceanography*, 41, 657–665, doi:10.1175/2010JPO4436.1, 2011.

455 Kobashi, F. and Kubokawa, A.: Review on North Pacific Subtropical Countercurrents and Subtropical Fronts: Role of mode waters in ocean circulation and climate, *Journal of Oceanography*, 68, 21–43, doi:10.1007/s10872-011-0083-7, 2012.

Large, W. G. and Yeager, S. G.: Diurnal to decadal global forcing for ocean and sea-ice models: {The} data sets and flux climatologies., NCAR Tech. Note, TN-460+ST, 105pp, doi:10.5065/D6KK98Q6, 2004.

460 Le Bars, D., Dijkstra, H. a., and De Ruijter, W. P. M.: Impact of the Indonesian throughflow on Agulhas leakage, *Ocean Science Discussions*, 10, 353–391, doi:10.5194/os-9-773-2013, <http://www.ocean-sci.net/9/773/2013/>, 2013.

Maltrud, M., Bryan, F., and Peacock, S.: Boundary impulse response functions in a century-long eddying global ocean simulation, *Environmental Fluid Mechanics*, 10, 275–295, doi:10.1007/s10652-009-9154-3, 2010.

465 McCreary, J. P., Shetye, S. R., and Kundu, P. K.: Thermohaline forcing of eastern boundary currents: With application to the circulation off the west coast of Australia, *Journal of Marine Research*, 44, 71–92, doi:10.1357/002224086788460184, 1986.

McCreary, J. P., Miyama, T., Furue, R., Jensen, T., Kang, H. W., Bang, B., and Qu, T.: Interactions between the 470 Indonesian Throughflow and circulations in the Indian and Pacific Oceans, *Progress in Oceanography*, 75, 70–114, doi:10.1016/j.pocean.2007.05.004, 2007.

Menezes, V. V., Phillips, H. E., Schiller, A., Domingues, C. M., and Bindoff, N. L.: Salinity dominance on the Indian Ocean Eastern Gyral current, *Geophysical Research Letters*, 40, 5716–5721, doi:10.1002/2013GL057887, 2013.

Merle, J., Rotschi, H., and Voituriez, B.: Zonal Circulation in the Tropical Western South Pacific at 170E, 475 Bulletin of the Japanese Society of Fisheries Oceanography, pp. 91–98, 1969.

Morrow, R. and Birol, F.: Variability in the southeast Indian Ocean from altimetry: forcing mechanisms for the Leeuwin Current, *Journal of Geophysical Research: Oceans*, 103, doi:10.1029/98JC00783, 1998.

Nauw, J. J., van Aken, H. M., Webb, a., Lutjeharms, J. R. E., and de Ruijter, W. P. M.: Observations of the southern East Madagascar Current and undercurrent and countercurrent system, *Journal of Geophysical Research: Oceans*, 113, 1–15, doi:10.1029/2007JC004639, 2008.

Palastanga, V., van Leeuwen, P. J., Schouten, M. W., and de Ruijter, W. P. M.: Flow structure and variability in the subtropical Indian Ocean: Instability of the South Indian Ocean countercurrent, *Journal of Geophysical Research: Oceans*, 112, 1–11, doi:10.1029/2005JC003395, 2007.

Pedlosky, J., Pratt, L. J., Spall, M. A., and Helfrich, K. R.: Circulation around islands and ridges, *Journal of Marine Research*, 55, 1199–1251, 1997.

Reid, J. L. and Mantyla, A. W.: On the Mid-Depth Circulation of the North Pacific Ocean, *Journal of Physical Oceanography*, 8, 946–951, doi:10.1175/1520-0485(1978)008<0946:OTMDCO>2.0.CO;2, 1978.

Ridgway, K. R. and Dunn, J. R.: Observational evidence for a Southern Hemisphere oceanic supergyre, *Geophysical Research Letters*, 34, 1–5, doi:10.1029/2007GL030392, 2007.

Schouten, M. W., de Ruijter, W. P. M., and Ridderinkhof, H.: A seasonal intrusion of subtropical water in the Mozambique Channel, *Geophysical Research Letters*, 32, 1–4, doi:10.1029/2005GL023131, 2005.

Smith, R. L., Huyer, A., Godfrey, J. S., and Church, J. a.: The Leeuwin Current off Western Australia, 1986–1987, doi:10.1175/1520-0485(1991)021<0323:TLCOWA>2.0.CO;2, 1991.

Song, Q., Gordon, A. L., and Visbeck, M.: Spreading of the Indonesian Throughflow in the Indian Ocean*, *Journal of Physical Oceanography*, 34, 772–792, doi:10.1175/1520-0485(2004)034<0772:SOTITI>2.0.CO;2, 2004.

Speich, S., Blanke, B., and Cai, W.: Atlantic meridional overturning circulation and the Southern Hemisphere supergyre, *Geophysical Research Letters*, 34, 1–5, doi:10.1029/2007GL031583, 2007.

Takeuchi, K.: Numerical Study of the Subtropical Front and the Subtropical Countercurrent*, *Journal of the Oceanographical Society of Japan*, 40, 371–381, 1984.

Tsuchiya, M.: Evidence of a double-cell subtropical gyre in the South Atlantic Ocean, *Journal of Marine Research*, 43, 57–65, doi:10.1357/002224085788437271, 1985.

Uda, M. and Hasunuma, K.: The Eastward Subtropical Countercurrent in the Western North Pacific Ocean, 25, 201–210, 1969.

Valsala, V. K. and Ikeda, M.: Pathways and effects of the Indonesian Throughflow water in the Indian Ocean using particle trajectory and tracers in an OGCM, *Journal of Climate*, 20, 2994–3017, doi:10.1175/JCLI4167.1, 2007.

van Sebille, E., Sprintall, J., Schwarzkopf, F. U., Gupta, A. S., Santoso, A., England, M. H., Biastoch, A., and Böning, C. W.: Pacific-to-Indian Ocean connectivity: Tasman leakage, Indonesian Throughflow, and the role of ENSO, pp. 1365–1382, doi:10.1002/2013JC009525. Received, 2014.

Waite, A., Thompson, P., Pesant, S., Feng, M., Beckley, L., Domingues, C., Gaughan, D., Hanson, C., Holl, C., Koslow, T., et al.: The Leeuwin Current and its eddies: An introductory overview, *Deep Sea Research Part II: Topical Studies in Oceanography*, 54, 789–796, 2007.

Weaver, A. J. and Middleton, J. H.: On the Dynamics of the Leeuwin Current, doi:10.1175/1520-0485(1989)019<0626:OTDOL>2.0.CO;2, 1989.

Weller, E., Holliday, D., Feng, M., Beckley, L., and Thompson, P.: A continental shelf scale examination of the Leeuwin Current off Western Australia during the austral autumn-winter, *Continental Shelf Research*, 31, 1858–1868, doi:10.1016/j.csr.2011.08.008, 2011.

520 Woo, M. and Pattiarchi, C.: Hydrography and water masses off the western Australian coast, *Deep-Sea Research Part I: Oceanographic Research Papers*, 55, 1090–1104, doi:10.1016/j.dsr.2008.05.005, 2008.

Woo, M., Pattiarchi, C., and Schroeder, W.: Dynamics of the Ningaloo Current off Point Cloates, Western Australia, *Marine and Freshwater Research*, 57, 291–301, doi:10.1071/MF05106, 2006.

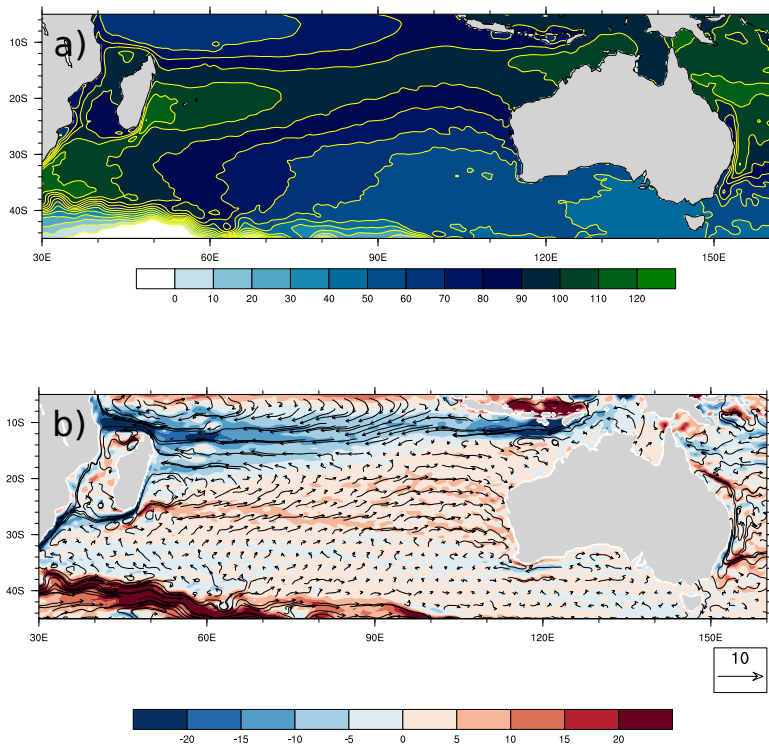


Figure 1. a) Mean dynamic topography (cm) from product *MDT_CNES-CLS13*. b) Derived geostrophic velocities (cms⁻¹), where positive values indicate an eastward component.

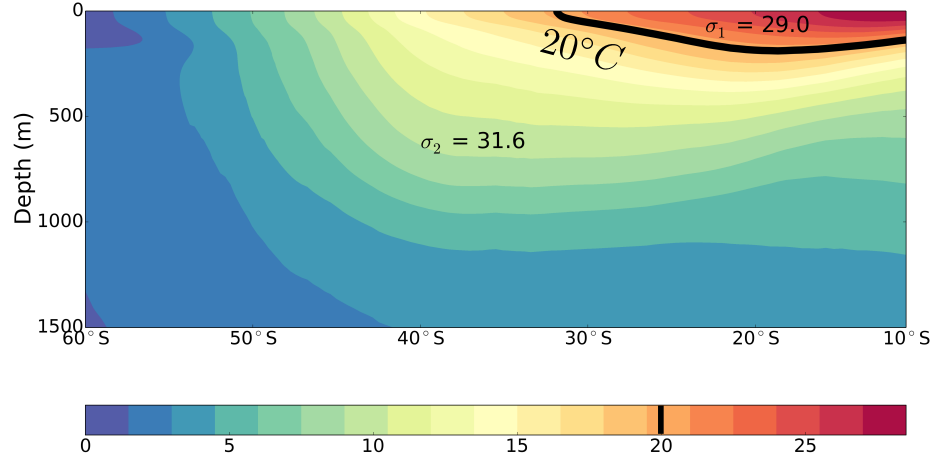


Figure 2. Meridional section of temperature ($^{\circ}\text{C}$) at 80°E from Argo floats (ARIVO project, Gaillard and Charraudeau (2008)). The 20°C isotherm is used to divide the basin into an upper and lower layer. For both layers, average relative densities σ are denoted, which are used for defining the stratification of the two-layer model. The isotherm shows outcrop near 30°S , marking the southern boundary of the upper layer.

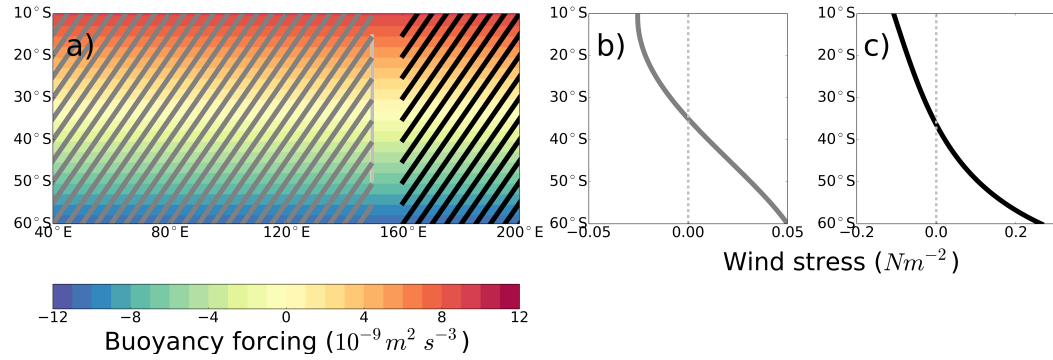


Figure 3. Configuration of the conceptual two-layer model. a) Model domain, applied buoyancy forcing (shading) and two areas where wind stress is applied (hatches). The light grey area at 150°E indicates the elongated island. b) Wind stress simulating a gyre (grey) and c) ITF (black) applied to respective areas as indicated in panel a).

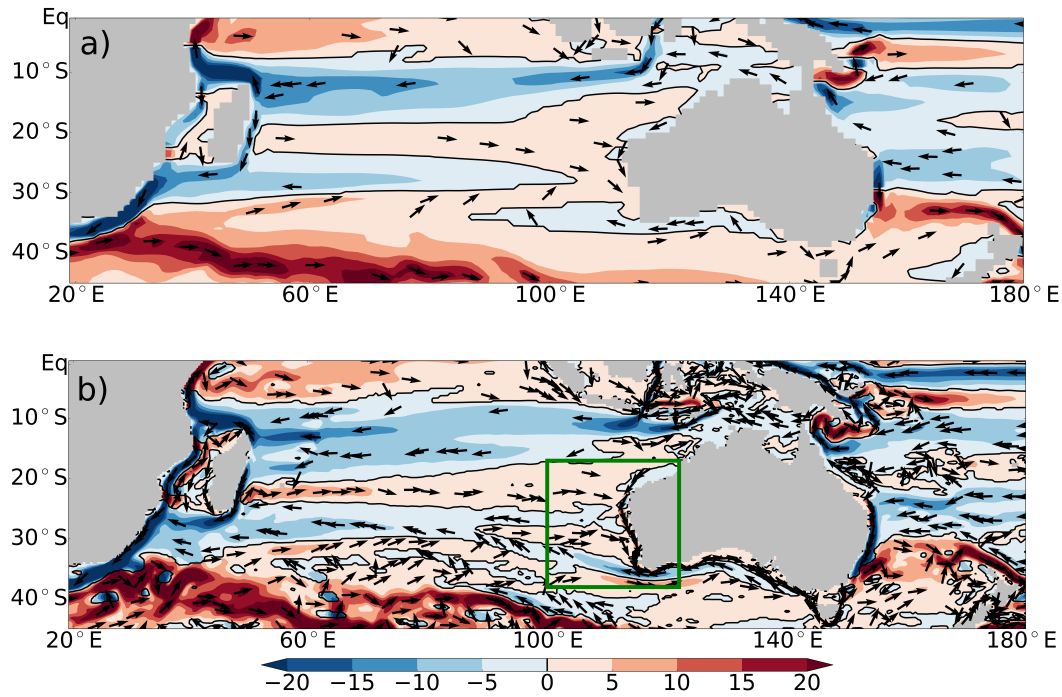


Figure 4. Steady-state horizontal velocities averaged over the top 200 m (cms^{-1}) from the GCM simulations. a) Coarse resolution (1.0°), b) eddy-resolving resolution (0.1°). Positive values indicate an eastward component. Unit vectors are added at local maxima to show the direction of the flow. The green box indicates the area shown in Fig. 5a.

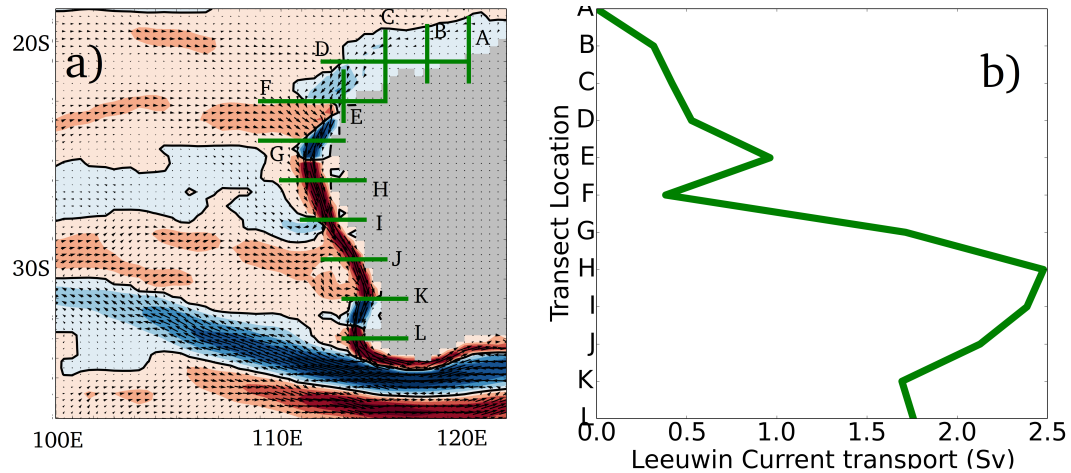
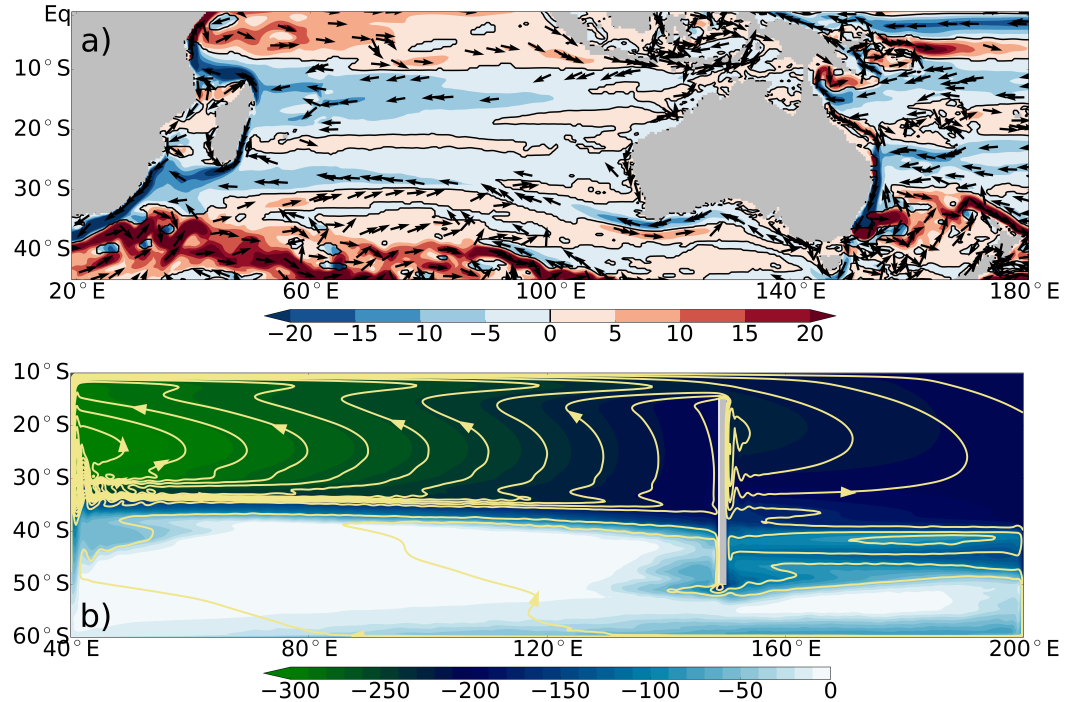


Figure 5. a) Inlet from Fig. 4 with indicated transects along the western coast. Transects are taken at intervals of 2° along the coast. Labels A-L are ordered from up- to downstream where A,B,C and E are meridional sections, the others zonal. b) Cross-transect velocities are integrated down to the depth of zero velocity to give an LC transport. This depth increases monotonically from 150 m at transect A to 300 m at transect L. Transect F marks the latitude of the North West Cape: 22°S .



Streamfunction (yellow contours, interval 1 Sv) of a) viscous and b) inertial circulation in the upper layer as forced by the configuration shown in Fig. 3 [without wind forcing in the eastern basin](#). Colour shading indicates the depth of the interface relative to the free surface in meters. [The white](#) [White](#) areas thus represent areas of (near-) outcrop.

Streamfunction (yellow contours, interval 1 Sv) of a) viscous and b) inertial circulation in the upper layer as forced by the configuration shown in Fig. 3 [without wind forcing in the eastern basin](#). Colour shading indicates the depth of the interface relative to the free surface in meters. [The white](#) [White](#) areas thus represent areas of (near-) outcrop.

Figure 6. a) As Fig. 4 with closed Indonesian Passages. b) [As Fig. 7 without the wind forcing in the eastern basin \(black hatches in Fig. 3\)](#).

Streamfunction (yellow contours, interval 1 Sv) of a) viscous and b) inertial circulation in the upper layer as forced by the configuration shown in Fig. 3 [without wind forcing in the eastern basin](#). Colour shading indicates the depth of the interface relative to the free surface in meters. [The white](#) [White](#) areas thus represent areas of (near-) outcrop.

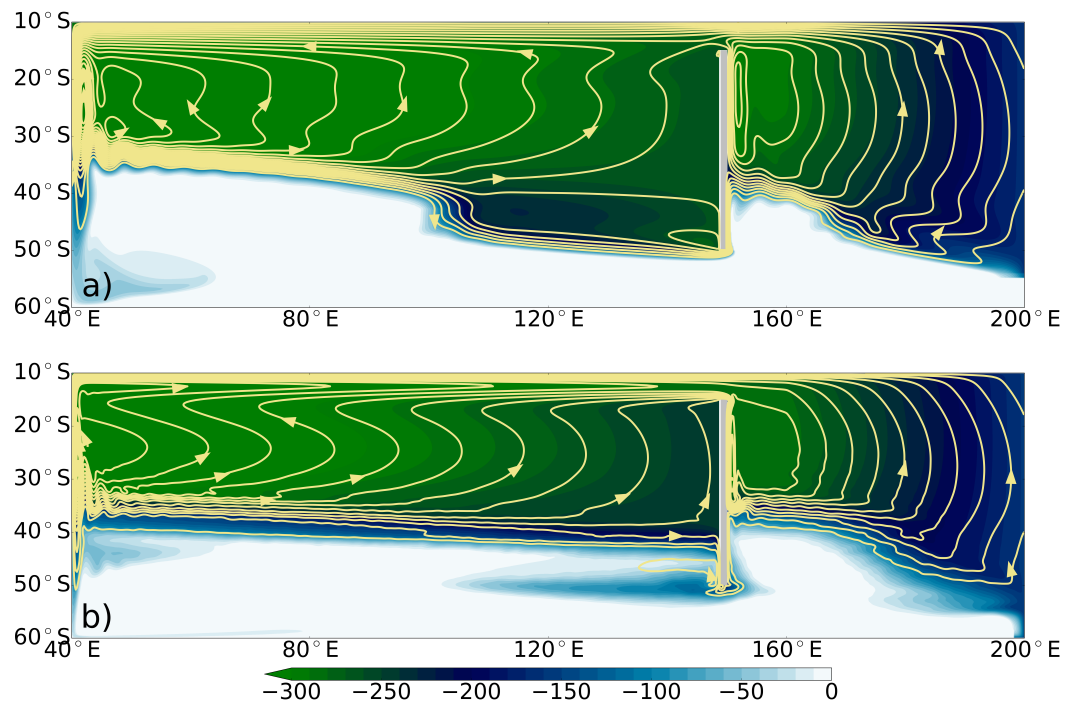


Figure 7. As Fig. 5 including wind forcing in the eastern basin for a) viscous and b) inertial circulation.